Development 140, 3413-3422 (2013) doi:10.1242/dev.094532

Inactivation of LAR family phosphatase genes *Ptprs* and *Ptprf* causes craniofacial malformations resembling Pierre-Robin sequence

Katherine Stewart[1], Noriko Uetani[1], Wiljan Hendriks[2], Michel L. Tremblay[1] and Maxime Bouchard[1,*]

SUMMARY

Leukocyte antigen related (LAR) family receptor protein tyrosine phosphatases (RPTPs) regulate the fine balance between tyrosine phosphorylation and dephosphorylation that is crucial for cell signaling during development and tissue homeostasis. Here we show that LAR RPTPs are required for normal development of the mandibular and maxillary regions. Approximately half of the mouse embryos lacking both *Ptprs* (RPTPσ) and *Ptprf* (LAR) exhibit micrognathia (small lower jaw), cleft palate and microglossia/glossoptosis (small and deep tongue), a phenotype closely resembling Pierre-Robin sequence in humans. We show that jaw bone and cartilage patterning occurs aberrantly in LAR family phosphatase-deficient embryos and that the mandibular arch harbors a marked decrease in cell proliferation. Analysis of signal transduction in embryonic tissues and mouse embryonic fibroblast cultures identifies an increase in Bmp-Smad signaling and an abrogation of canonical Wnt signaling associated with loss of the LAR family phosphatases. A reactivation of β-catenin signaling by chemical inhibition of GSK3β successfully resensitizes LAR family phosphatase-deficient cells to Wnt induction, indicating that RPTPs are necessary for normal Wnt/β-catenin pathway activation. Together these results identify LAR RPTPs as important regulators of craniofacial morphogenesis and provide insight into the etiology of Pierre-Robin sequence.

KEY WORDS: LAR phosphatases, Craniofacial development, Bmp, Wnt, Pierre-Robin sequence, Mouse

INTRODUCTION

Pierre-Robin sequence (PRS) is a craniofacial malformation characterized by defects in mandibular development, which result in micrognathia (smaller lower jaw), glossoptosis (backward displacement of the tongue) and cleft palate (OMIM: 261800) (Robin, 1934; Izumi et al., 2012). Ultimately, PRS results in severe respiratory distress and feeding difficulties postnatally (Evans et al., 2011; Mackay, 2011; Izumi et al., 2012). This developmental phenotype can occur concurrent to, or separately from, additional syndromic malformations (Sheffield et al., 1987; Printzlau and Andersen, 2004; Izumi et al., 2012).

In the developing embryo, the mandible (lower jaw and anterior tongue) and the maxillary (upper jaw and palate) are derivatives of the first pharyngeal arch (PA1) (Santagati and Rijli, 2003; Yoshida et al., 2008; Gitton et al., 2010). The pharyngeal arches are segmented structures of the embryonic head composed of a mesodermal core surrounded by neural crest cell (NCC)-derived mesenchyme and encapsulated in ectodermal and endodermal epithelium (Santagati and Rijli, 2003; Minoux and Rijli, 2010). Both the epithelial and mesenchymal components of the arches directly contribute to their development and patterning through bidirectional signaling crosstalk that controls the proliferation, survival and differentiation of NCC-derived mesenchyme (Clouthier et al., 1998; Thomas et al., 1998; Hu and Helms, 1999; Abu-Issa et al., 2002; Abzhanov and Tabin, 2004; Liu et al., 2005; Haworth et al., 2007; Hu and Marcucio, 2009; Reid et al., 2011; Wang et al., 2011). Mandibular outgrowth from PA1 is a prerequisite for the appropriate morphogenesis of additional structures, including the tongue and palate. Lengthening of the mandible provides the impetus for the developing tongue to lower, thus allowing the palatal shelves to elevate horizontally above the tongue and eventually fuse, separating the oral cavity from the nasopharynx (Ricks et al., 2002). A failure in this series of events leads to PRS, which occurs in 1:8500 to 1:14,000 infants (Benko et al., 2009; Izumi et al., 2012).

The initial outgrowth of PA1 results from the combined activity of sonic hedgehog and canonical Wnt signaling (Yamaguchi et al., 1999; Brault et al., 2001; Jeong et al., 2004; Jin et al., 2011; Lin et al., 2011; Zhang et al., 2011; Sun et al., 2012). Importantly, conditional inactivation of β-catenin in PA1 mesenchyme leads to a severe reduction in mandibular growth, despite normal NCC migration and establishment within PA1 (Brault et al., 2001). In addition, specific loss of β-catenin activity in the mandibular epithelium results in partial reprogramming of the underlying mesenchyme, leading to the formation of a rudimentary lower jaw (Jin et al., 2011; Sun et al., 2012).

Additional pathways required to specify the identity of mesenchymal cells within PA1 include endothelin, fibroblast growth factor (FGF) and bone morphogenetic protein (BMP) signaling (Santagati and Rijli, 2003; Minoux and Rijli, 2010). In particular, loss or gain of BMP pathway activity results in dysregulated mandibular epithelial/mesenchymal signaling, leading to an undersized PA1 and the truncation of the mandibular region (Stottmann et al., 2001; Ishii et al., 2005; Liu et al., 2005; Bonilla-Claudio et al., 2012). BMP signaling is also implicated in the timing of cranial neural crest-derived mandibular bone and cartilage differentiation during craniofacial development (Liu et al., 2005; Merrill et al., 2008; Bonilla-Claudio et al., 2012).

Receptor protein tyrosine phosphatases (RPTPs) of the mammalian leukocyte antigen related (LAR) family comprise three genes: *Ptprd* (RPTPδ), *Ptprs* (RPTPσ) and *Ptprf* (LAR) (Chagnon

[1]Goodman Cancer Research Centre, Department of Biochemistry, McGill University, Montreal, 1160 Pine Avenue W. Montreal, QC H3A 1A3, Canada. [2]Department of Cell Biology, Nijmegen, Radboud University Nijmegen Medical Centre, PO Box 9101, 6500 HB Nijmegen, The Netherlands.

*Author for correspondence (maxime.bouchard@mcgill.ca)

Accepted 12 June 2013

et al., 2004; Hendriks et al., 2013). LAR family phosphatases have been implicated in several key embryonic signaling pathways, including those involved in the negative regulation of growth factor receptors such as EGFR, RET and MET, and potentially modulate canonical Wnt/β-catenin signaling (Kypta et al., 1996; Müller et al., 1999; Tisi et al., 2000; Wang et al., 2000; Ensslen-Craig and Brady-Kalnay, 2004; Machide et al., 2006; Haapasalo et al., 2007; Uetani et al., 2009; Zheng et al., 2011). Although LAR family phosphatases are expressed in several embryonic and adult tissues (Schaapveld et al., 1998), mice mutant for single family members generally survive to adulthood, reflecting a functional redundancy within the family (Schaapveld et al., 1997; Elchebly et al., 1999; Wallace et al., 1999; Uetani et al., 2000; Thompson et al., 2003; Wang et al., 2011). Accordingly, *Ptprd;Ptprs* double-mutant embryos show defects in motoneuron innervation (Uetani et al., 2006), whereas *Ptprs;Ptprf* double-mutants harbor severe urogenital and craniofacial defects (Uetani et al., 2009). Although micrognathia and cleft palate were noted in approximately half of *Ptprs;Ptprf* double-knockout (DKO) embryos at embryonic day (E) 18.5 (Uetani et al., 2009), the molecular and cellular basis for this phenotype was not investigated further. In this study, we demonstrate that *Ptprs* and *Ptprf* are necessary for mandibular morphogenesis through the regulation of Wnt and Bmp signaling, and that their absence results in a phenotype closely resembling PRS.

MATERIALS AND METHODS

Mice

The derivation of genetically modified *Ptprs;Ptprf* mice has been described (Uetani et al., 2009). All *Ptprs;Ptprf* embryos were generated in a C57Bl/6 genetic background. Throughout, control embryos were taken as $Ptprs^{+/-};Ptprf^{+/+}$ or $Ptprs^{+/+};Ptprf^{+/-}$, both of which are phenotypically normal. Derivation of *Ptprs;Ptprd:Ptprf* mutant mice used to generate triple-knockout embryonic fibroblasts will be described elsewhere. Mice were kept under pathogen-free conditions at the Animal Resources Centre of McGill University. Timed matings were performed and detection of copulatory plugs was taken as E0.5. All experiments involving mice were approved by the McGill Animal Care Committee and were performed according to the Canadian Council of Animal Care ethical guidelines for animal experiments.

Skeletal preparation

Skeletons of E14.5 or E18.5 embryos were stained with Alcian Blue and Alizarin Red as described (McLeod, 1980). Briefly, embryos from timed matings were fixed in 95% ethanol, fat was removed in 100% acetone, and the remaining bone and cartilage were stained in a solution of 0.015% Alcian Blue 8GS (Sigma), 0.005% Alizarin Red S (Sigma), 5% acetic acid, 70% ethanol for 3 days at 37°C. Skeletons were washed in water before clearing through a glycerol/potassium hydroxide gradient and stored in 100% glycerol for imaging. Images were acquired on a Zeiss Stemi 2000C/AxioCam MRc dissecting microscope and camera.

In situ hybridization

Embryo dissections and processing, as well as whole-mount and section *in situ* hybridizations, were performed as described (Grote et al., 2008). Probes for *Ptprf* and *Ptprs* have been described (Uetani et al., 2009). Probes for *Crabp1*, *Col2a1*, *Runx2* and *Msx1* were generated from E11.5 whole-embryo cDNA using specific primers (supplementary material Table S1). The resultant PCR products were cloned into the pGEM-T Easy vector (Promega) and transcribed following standard procedures using SP6 or T7 RNA polymerase and DIG-labeled dNTPs (Roche).

Immunohistological staining

Hematoxylin and Eosin (H&E) staining of control and double-mutant embryos was performed as described (Uetani et al., 2009). For immunohistological stainings, tissues were fixed in 4% paraformaldehyde (PFA) in PBS at 4°C overnight, embedded in OCT compound (Sakura Finetek), and cryosectioned at 12 μm. Alternatively, treated mouse embryonic fibroblasts (MEFs) were fixed in 4% PFA in PBS for 20 minutes at room temperature, and rinsed twice with PBS. Samples were permeabilized with 0.25% Triton X-100 in PBS for 5-10 minutes, blocked with DAKO Protein Block (serum-free) solution for 1 hour at room temperature and incubated with the following antibodies: rabbit anti-phospho-histone H3 (1:400, Millipore), rabbit anti-β-catenin (1:500, Millipore), mouse anti-dephosphorylated β-catenin (1:100, Millipore), rabbit anti-phosphorylated SMAD1/5 (1:50, Cell Signaling Technology) and mouse anti-CRABP1 (1:200, Abcam). Secondary detection employed anti-rabbit or anti-mouse secondary antibodies labeled with Alexa Fluor 488 or Alexa Fluor 568 (1:400, Invitrogen). Samples were counterstained with Alexa Fluor 546-labeled phalloidin (1:400, Invitrogen) and/or DAPI (50 μg/ml, Invitrogen). For apoptotic index, sections were labeled by TUNEL using the *In Situ* Cell Death Detection Kit (Roche) according to the manufacturer's instructions. All fluorescent stainings were mounted in SlowFade Gold mounting medium (Invitrogen), and images were acquired using a Zeiss AxioPlan 2 microscope or a Zeiss LSM 5 Pascal/Axiovert 200M confocal microscope.

Cell culture

MEFs were derived from control and *Ptprs;Ptprd;Ptprf* triple-knockout embryos at E13.5 by standard procedures. Briefly, embryos were dissected in PBS, the internal organs removed, and the connective tissue trypsinized to a single-cell suspension at 37°C. Trypsinization was stopped with 10% fetal bovine serum (FBS; Wisent) in DMEM medium, and mesenchymal cells were allowed to adhere in 10-cm plates. After 8 hours the plates were washed with PBS to detach non-mesenchymal cells. Cells were maintained in DMEM medium supplemented with 10% FBS and penicillin-streptomycin (Invitrogen) until passage five, when they were used experimentally. For immunofluorescent staining, cells were seeded on acid-washed glass coverslips and allowed to adhere overnight prior to treatment. Cells were treated with 100 ng/ml recombinant mouse BMP4 or recombinant human WNT3A for 30 minutes, following which protein was collected or cells were fixed. For experiments involving the GSK inhibitor, cells were treated with 3 μM (2′Z,3′E)-6-bromoindirubin-3′-oxime (BIO; EMD) for 30 minutes prior to fixation or RNA extraction.

Immunoblotting

MEFs were treated with the indicated chemicals, and then rinsed with PBS twice. Protein was extracted on ice using RIPA buffer containing NaF, $NaVO_4$ and EDTA-free Complete Protease Inhibitors (Roche). Protein concentration was calculated using the Bradford Assay Kit (Bio-Rad), and 30-50 μg protein was run on an SDS-PAGE gel. Protein was transferred to PDVF membranes and blotted by standard methods. Antibody dilution and blocking were as recommended by the manufacturers. Antibodies used were anti-phospho-SMAD1/5 and anti-SMAD1 (Cell Signaling Technology), anti-α-tubulin (Abcam), and HRP-conjugated anti-mouse secondary (Santa Cruz) or HRP-conjugated anti-rabbit secondary (Abcam) antibodies. Signal was detected using the Immobilon Western Chemiluminescent HRP Substrate Kit (Millipore). When necessary, blots were stripped with ReBlot Plus Strong solution (Millipore) prior to reblotting with a different antibody.

Real-time quantitative PCR

MEFs were treated with the indicated chemicals in triplicate, rinsed with PBS, and RNA was extracted with Trizol (Invitrogen) following standard procedures. Alternatively, the first branchial arches were dissected from E10.5 embryos in ice-cold DEPC-treated PBS and immediately resuspended in Trizol. We used 1 μg of RNA to generate cDNA using SuperScript III reverse transcriptase (Invitrogen). Quantitative PCR (qPCR) was performed on Eppendorf Realplex2 cyclers using the iQ SYBR Green Supermix Kit (Bio-Rad). The mouse β2-microglobulin (*B2m*), *Axin2*, cyclin D1 (*Ccnd1*), *Ptc1*, *Msx1*, *Dlx1*, *Dlx5*, *Gsc*, *Sox9*, *Col2a1* and *Runx2* primers are listed in supplementary material Table S1. All samples were run in technical triplicates, and transcript levels were standardized using *B2m*. Expression levels for control and treated samples were compared with each biological triplicate using the delta-delta qPCR method to capture biological variance between samples (Pfaffl, 2001).

Image analysis and statistics

Proliferative and apoptotic indices were determined using the Measure function in the Zeiss AxioVision 4 image acquisition program. Cell counting was performed on six sections spanning the mandibular arch in each of three controls and three affected double-mutant embryos between E10.5 and E12.5 using Adobe Photoshop. Statistical analyses were performed using unpaired two-tailed Student's *t*-tests. Data are presented as mean ± s.e.; $P<0.05$ was considered significant.

RESULTS

Craniofacial skeletal malformations in *Ptprs*$^{-/-}$;*Ptprf*$^{-/-}$ embryos

We have previously reported a requirement for the LAR family members *Ptprs* (RPTPσ) and *Ptprf* (LAR) in craniofacial morphogenesis (Uetani et al., 2009). In particular, approximately half of the embryos lacking *Ptprs;Ptprf* exhibit micrognathia and cleft palate at E18.5, defects that are not observed in the other genotypes of the allelic series. As these are common craniofacial abnormalities in infants, we undertook a detailed characterization of this phenotype.

To visualize gross malformations of the mouse skeleton we first performed Alizarin Red and Alcian Blue staining, which identifies mineralized bones and cartilage, respectively. An analysis of the torso and limb skeletal elements failed to reveal any significant alterations in the double-mutant embryos (supplementary material Fig. S1A,B). By contrast, evaluation of skull preparations from *Ptprs*$^{-/-}$;*Ptprf*$^{-/-}$ and control embryos at E18.5 revealed defects in calvarial development, including abnormal frontal and parietal bones, an absence of the nasal capsule, and truncation of the premaxilla, although the maxilla appeared grossly normal (Fig. 1A,B). Furthermore, loss of *Ptprs* and *Ptprf* resulted in dysmorphogenesis of the oral cavity, as double-mutant embryos lack palatine bones, which, together with a dysmorphic basiosphenoid and absent pterygoid processes, are consistent with cleft palate (Fig. 1C,D). Strikingly, *Ptprs*$^{-/-}$;*Ptprf*$^{-/-}$ embryos harbored severe defects in mandibular morphogenesis. In comparison to age-matched littermates, affected DKO mandibles were narrower and shortened, with aberrant bone deposition between the dentary bones (Fig. 1E,F). Additionally, the distal symphysis was fused at the midline in double-mutant mandibles, whereas the rostral processes (angular, coronoid, condylar) were present, suggesting that the proximal mandible was patterned correctly (Fig. 1E,F). The mandibular hypoplasia and cleft palate were clearly visible in E18.5 coronal sections stained with H&E (Fig. 1G,H). These sections additionally revealed that the DKO embryos had a small tongue (microglossia) located further back in the oral cavity (glossoptosis) (Fig. 1I,J). This shift was accompanied by a marked reduction in airway space (Fig. 1I,J).

The striking triad of micrognathia, glossoptosis and cleft palate in embryos lacking LAR family phosphatases prompted us to more rigorously investigate their association during mandibular development. In accordance with our previous investigation (Uetani et al., 2009), 39% of *Ptprs*$^{-/-}$;*Ptprf*$^{-/-}$ embryos harbored micrognathia. Notably, all of these embryos also exhibited microglossia and palatal defects, including cleft palate and palatal bone abnormalities at E16.5 and E18.5 ($n=7$). All micrognathic *Ptprs*$^{-/-}$;*Ptprf*$^{-/-}$ embryos analyzed also had glossoptosis. Conversely, *Ptprs*$^{-/-}$;*Ptprf*$^{-/-}$ embryos without micrognathia had normal tongues and palates ($n=11$). In addition, neither controls nor embryos with a single allele of either *Ptprs* or *Ptprf* displayed these defects ($n=35$), highlighting the strong association between the defects in mandible, tongue and palatal shelf development in the affected double mutants. Together, these defects comprise the morphological features of PRS.

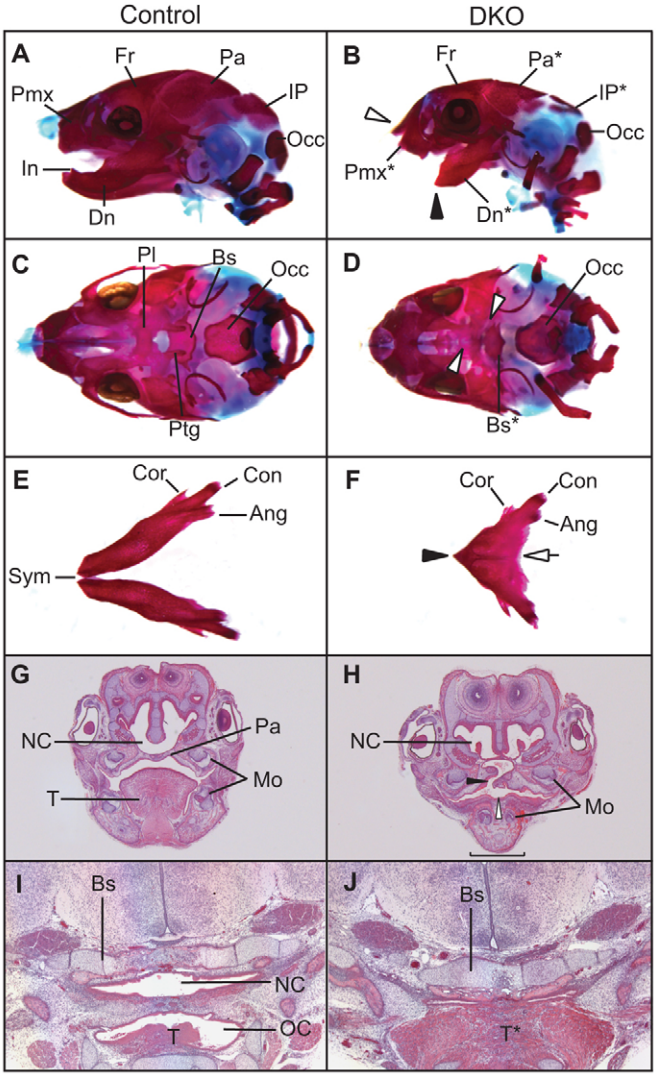

Fig. 1. Defects in the craniofacial morphology of *Ptprs*$^{-/-}$;*Ptprf*$^{-/-}$ mouse embryos at E18.5. (**A-F**) Alizarin Red and Alcian Blue stainings of bone and cartilage from control and *Ptprs;Ptprf* double-knockout (DKO) embryos at E18.5. Note the significant defects in maxillary (B,D, white arrowheads) and mandibular (B,F black arrowheads) development, with absent palatal bones and a severely dysmorphic dentary bone (F, white arrow). (**G-J**) H&E stainings of E18.5 coronal sections. (G,H) Anterior sections reveal the presence of cleft palate (black arrowhead) and the absence of a differentiated tongue concomitant with micrognathia (white arrowhead) in the mutant. (I,J) Posterior sections show the backward displacement of a disorganized tongue in *Ptprs*$^{-/-}$;*Ptprf*$^{-/-}$ mutants, accompanied by blockage of the oral cavity. Asterisks indicate the dysmorphic mutant phenotype. Ang, angular process; Bs, basisphenoid; Con, condylar process; Cor, coronoid process; Dn, dentary bone; Fr, frontal bone; In, lower incisor; IP, interparietal bone; Mo, molars; NC, nasal cavity; OC, oral cavity; Occ, occipital bone; Pa, palate; Pl, palatine; Pmx, premaxilla; Ptg, pterygoid; Sym, distal symphis of mandible; T, tongue.

Ptprs$^{-/-}$;*Ptprf*$^{-/-}$ embryos show a patterning defect in cartilage and bone deposition

To investigate the origin of the craniofacial skeletal defects observed in *Ptprs*$^{-/-}$;*Ptprf*$^{-/-}$ embryos, we characterized the onset of

craniofacial bone ossification. Consistent with the E18.5 skeletal analysis, Alizarin Red and Alcian Blue staining at E14.5 revealed that appendicular bones and cartilages were normal in *Ptprs*$^{-/-}$;*Ptprf*$^{-/-}$ embryos (supplementary material Fig. S1C,D). However, E14.5 DKO embryos were already identifiable as having an undersized lower jaw and lacking a tongue (Fig. 2A,B; data not shown). Cranial bone and cartilage tissues were dysmorphic, including shortened cartilage anlagen of the premaxilla and nasal capsule (Fig. 2C,D). Most strikingly, *Ptprs*$^{-/-}$;*Ptprf*$^{-/-}$ embryos had a dysplastic Meckel's cartilage, with foreshortened and mispatterned middle processes that were aberrantly fused at the distal tip (Fig. 2E,F), while the proximal arms articulated correctly with the middle ear capsule (supplementary material Fig. S1E,F). Furthermore, mandibular bone deposition occurred medially in double-mutant embryos in comparison with control mandibles, resulting in premature fusion of the dentary bones (Fig. 2E,F). Together, these results identify a role of LAR family phosphatases in the patterning of mandibular cartilage and bone structures.

The inappropriate morphogenesis of Meckel's cartilage and mandibular bone suggested a possible misspecification of precursor cell populations at earlier time points. Differentiation of mesenchymal cells to chondrocytes and osteoblasts that lay down Meckel's cartilage and dentary bone initiates at ~E12.5 in the mouse (Ito et al., 2002). Early chondrocytic populations are marked by the expression of collagen 2α1 (Zhao et al., 1997), whereas osteoblast lineages are specified by the transcription factor Runx2 (Funato et al., 2009). To assess the integrity of chondrocyte and osteoblast cell populations in the developing mandibular process, we performed *in situ* hybridization for *Col2a1* and *Runx2* transcripts on coronal sections of control and *Ptprs*$^{-/-}$;*Ptprf*$^{-/-}$ embryos. Strikingly, whereas *Col2a1* and *Runx2* expression is only just beginning in the distal mandibular arch of wild-type embryos at E12.5, *Ptprs*$^{-/-}$;*Ptprf*$^{-/-}$ embryos exhibit aberrant midline expression of both lineage markers at this stage (Fig. 2G-J). In the proximal mandible, *Col2a1* and *Runx2* stainings revealed that the cartilage condensations and surrounding osteoblast populations were unchanged in the DKO embryos as compared with controls (supplementary material Fig. S2). This marker analysis is in line with the aberrant fusion of Meckel's cartilage and mandibular bone at later embryonic stages.

Ptprs;Ptprf deficiency affects mandibular cell proliferation

To determine the origin of the mandibular patterning defect observed in the double-mutant embryos we first asked whether it was a result of defective cranial NCC migration into the pharyngeal arches. We performed whole-mount *in situ* hybridization and immunofluorescence with the NCC marker CRABP1 at E9.5, which revealed a similar migratory pattern in control and *Ptprs*$^{-/-}$;*Ptprf*$^{-/-}$ embryos (supplementary material Fig. S3A-D). TUNEL staining of migratory NCCs also failed to show any difference in NCC survival (supplementary material Fig. S3C-E). Together, these results argue against a defect in the delamination, migration or survival of cranial NCCs in LAR family-deficient embryos.

We next investigated whether apoptosis and proliferation were affected within the pharyngeal arches at later time points. As observed with NCCs, TUNEL staining of mandibular tissue failed to reveal any significant change in cell survival between mutant and control embryos (Fig. 3A,B; data not shown). By contrast, embryos lacking RPTP-σ and LAR exhibited a marked decrease in proliferation throughout PA1 and the developing oral cavity, as shown by immunostaining for the mitotic marker phospho-histone H3 (Fig. 3A-K). Specifically, *Ptprs*$^{-/-}$;*Ptprf*$^{-/-}$ embryos had ~70% reduction in pharyngeal arch cell proliferation at E10.5 (Fig. 3A-C), a defect that was largely maintained in the proximal arch of E12.5 DKO embryos, whereas proliferation in the distal mandibular arch more closely resembled control levels (Fig. 3D-G,J). Additionally, cell proliferation in the developing tongue and palatal shelves of *Ptprs*$^{-/-}$;*Ptprf*$^{-/-}$ embryos at E12.5 was reduced to ~50% of control levels (Fig. 3H-J), potentially further contributing to the later developmental defects observed in these tissues.

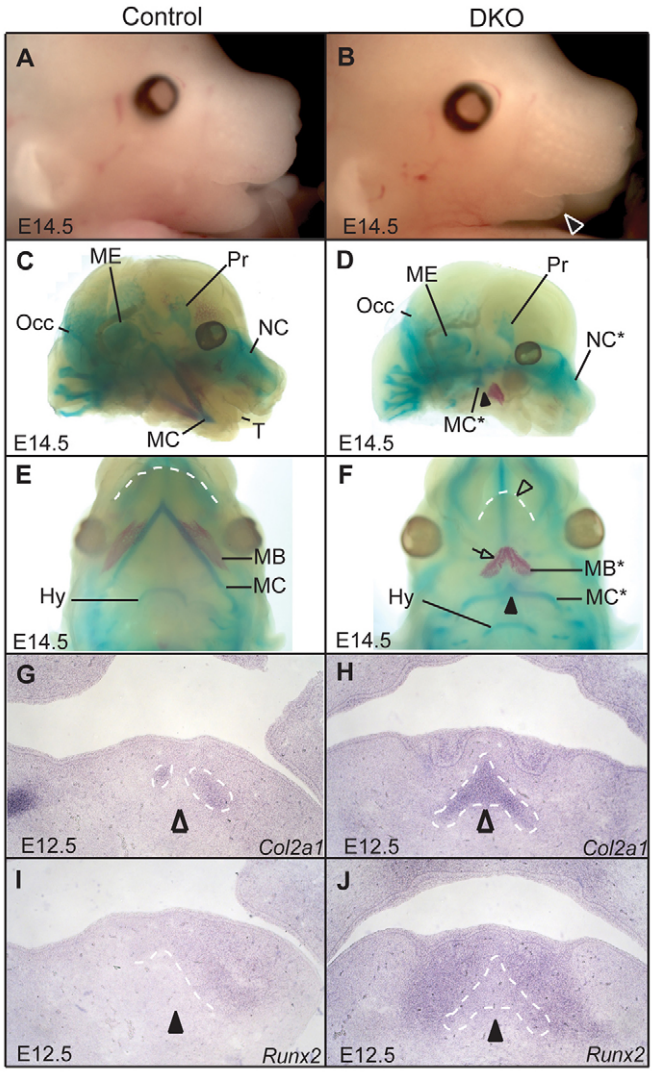

Fig. 2. Bone and cartilage defects of *Ptprs*$^{-/-}$;*Ptprf*$^{-/-}$ mouse embryos. (**A**,**B**) Control and DKO embryos prior to staining at E14.5. Note the severely undersized jaw and absent tongue in the mutant (arrowhead). (**C-F**) Alizarin Red and Alcian Blue stainings of bone and cartilage at E14.5. Meckel's cartilage (D,F, black arrowheads) and mandibular bone (F, open arrow) are dysmorphic at E14.5. Also apparent is the shortened, narrowed lower jaw in E14.5 DKO embryos (F, open arrowhead). (**G-J**) *In situ* hybridization of coronal sections at E12.5. (G,H) In contrast to controls, DKO embryos show aberrant specification of the *Col2a1* chondrocyte marker (open arrowheads) in the medial mandibular arch. (I,J) Similarly, aberrant specification of the *Runx2* osteoblast marker (black arrowheads) occurs in DKO embryos. Asterisks indicate the dysmorphic mutant version. Dashed lines indicate the lower jaw (E,F) and Meckel's cartilage precursors (G-J), respectively. Hy, hyoid cartilage; MB, mandibular bone; MC, Meckel's cartilage; ME, middle ear; NC, nasal capsule; Pr, parietal bone; other labels as Fig. 1.

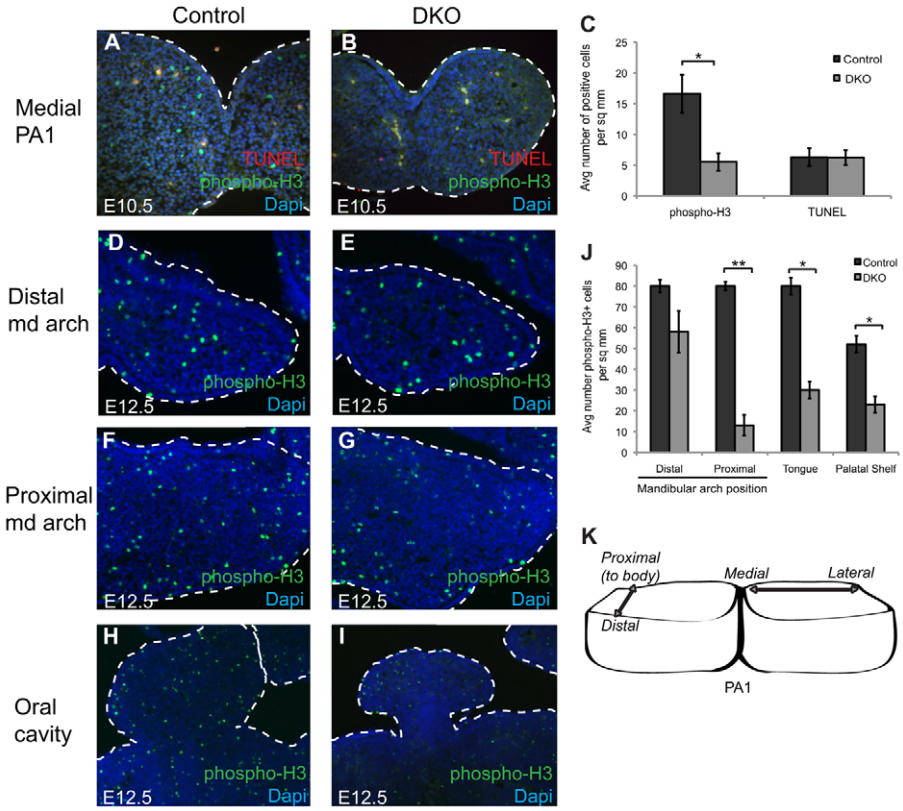

Fig. 3. *Ptprs*$^{-/-}$;*Ptprf*$^{-/-}$ mouse embryos exhibit a decrease in cell proliferation in the mandibular arch. (**A-C**) Immunofluorescent labeling (A,B) and cell counts (C) of TUNEL^{+} and phospho-histone H3^{+} cells on coronal first pharyngeal arch (PA1) sections at E10.5. DKO embryos show a significant reduction in proliferating cells, whereas no significant difference in apoptotic cell index is observed. (**D-J**) Immunofluorescent labeling and cell counts of TUNEL^{+} and phospho-histone H3^{+} cells on coronal mandibular (md) arch and oral cavity sections at E12.5. Note that the strong reduction in the proliferation of DKO mandibular arch cells is maintained. In addition, proliferation is impaired in mutant tongue and palatal shelf tissue. (**K**) Schematic of the mandibular arch indicating the proximal-distal and medial-lateral axes. PA1, first branchial arch. Error bars indicate s.e.; **P*<0.05, ***P*<0.01.

Ptprf and *Ptprs* are co-expressed in the distal mandibular process

The developmental defects observed in double-mutant embryos raised the question of where LAR family phosphatases act in the developing mandibular and maxillary processes. To address this we determined the mRNA expression patterns of *Ptprf* and *Ptprs* by *in situ* hybridization throughout early craniofacial development. Interestingly, at E9.5-10.5 *Ptprf* was strongly expressed in the distal epithelium and mesenchyme of PA1 but expressed at lower levels in the proximal regions (Fig. 4A,B). Conversely, *Ptprs* was more diffusely expressed throughout the PA1 mesenchyme and was absent from the distal epithelium (Fig. 4D,E). At E12.5, *Ptprf* was expressed at relatively low levels in the mandibular arch mesenchyme and at higher levels throughout the oral epithelium, whereas *Ptprs* was expressed at similar levels in both compartments (Fig. 4C,F). This expression continued at E15.5, as *Ptprf* was expressed in the oral epithelium and palatal seam, which is the site of secondary palatal shelf fusion, whereas *Ptprs* was only weakly expressed in the seam region at this stage (supplementary material Fig. S4A-D). Hence, the expression patterns of *Ptprf* and *Ptprs* align well with a role in patterning the developing pharyngeal arch, and might suggest a later role in palatal shelf morphogenesis.

Wnt and Bmp signaling pathways are dysregulated in *Ptprs;Ptprf*-deficient cells

Much of the cellular behavior within PA1, including survival, proliferation and differentiation, is dictated by reciprocal signaling between the epithelial and mesenchymal compartments (Santagati and Rijli, 2003; Minoux and Rijli, 2010). To identify the molecular alterations caused by *Ptprs;Ptprf* deficiency, we characterized several signaling pathways involved in pharyngeal arch morphogenesis at E10.5. Given the stronger distal expression of *Ptprs* and *Ptprf* in the developing pharyngeal arch, we first asked whether distal epithelial signaling of the BMP pathway was perturbed upon loss of PPTP-σ and LAR. We examined the downstream signaling effector phosphorylated (p) SMAD1/5 by immunofluorescence. This experiment revealed an increase in pSMAD1/5 signal in the distal mesenchyme of double mutants, suggesting that the BMP signaling pathway is overactive in the *Ptprs*$^{-/-}$;*Ptprf*$^{-/-}$ PA1 (Fig. 5A,B). To confirm this, we performed *in situ* hybridization for the BMP-regulated gene *Msx1* on E10.5 transverse sections. In control embryos *Msx1* is expressed normally in the medial-distal region of the pharyngeal arch, whereas expression is expanded proximal-laterally upon loss of the LAR family phosphatases (Fig. 5C,D). The specific increase in BMP signaling was further confirmed by RT-qPCR analysis of dissected PA1, which indeed demonstrated an upregulation of *Msx1* in DKO embryos, whereas target genes of endothelin 1 and FGF signaling were unchanged (Fig. 5E). Intriguingly, the area of increased BMP signaling preceded the aberrant chondrogenesis and osteogenesis observed in the distal arch.

To confirm the effect of LAR family phosphatase deficiency on BMP signaling we used primary mouse embryonic fibroblasts (MEFs) deficient for *Ptprs*, *Ptprf* and the third LAR family member, *Ptprd*. These triple-knockout (TKO) MEFs were used instead of *Ptprs*$^{-/-}$;*Ptprf*$^{+/-}$ MEFs to avoid functional compensation by RPTP-δ, which is not normally expressed in the mandibular arch (data not shown). In the absence of ligand, a weak activation of pSMAD1/5 was observed specifically in LAR family-deficient cells (Fig. 5F,G). In response to recombinant (r) BMP4 treatment, TKO MEFs showed a marked upregulation and more efficient nuclear localization of pSMAD1/5 as detected by immunofluorescence (Fig. 5H,I). This result was confirmed by western blot analysis, which showed a strong increase in pSMAD1/5 signal in TKO MEFs as compared with wild type, while total SMAD1 levels remained unchanged (Fig. 5J). Furthermore, *in vitro* analysis of the BMP

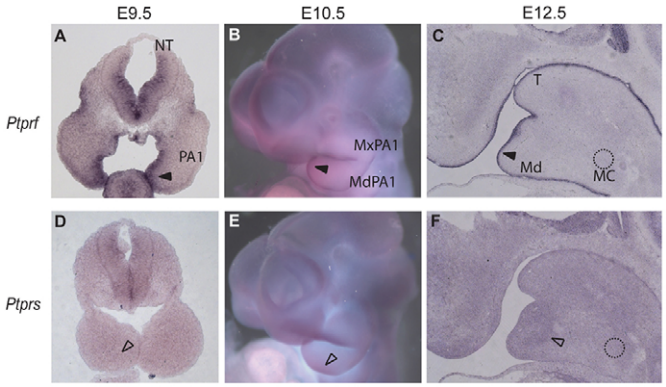

Fig. 4. Expression patterns of *Ptprf* and *Ptprs* during PA1 development and differentiation. *In situ* hybridization using probes for (**A-C**) *Ptprf* and (**D-F**) *Ptprs* during PA1 development between E9.5 and E12.5. *Ptprf* is expressed strongly in the epithelial compartments and distal mesenchyme of the mandibular arch. *Ptprs* is co-expressed in the mesenchyme, and more diffusely in the epithelia. Arrowheads indicate regions of significant expression. Md, mandible; NT, neural tube; MdPA1, mandibular pharyngeal arch; MxPA1 maxillary pharyngeal arch; other abbreviations as Figs 1 and 2.

signaling response revealed an upregulation of both the chondrocytic genes *Sox9* and *Col2a1* and the osteoblast gene *Runx2* in wild-type fibroblasts upon rBMP4 stimulation (Fig. 5K). Strikingly, TKO cells were further sensitized to BMP ligand, as they upregulated both chondrocytic and osteoblast markers by 2- to 12-fold over the wild-type fibroblast response (Fig. 5K). These results suggest that LAR family phosphatases dampen BMP signaling in mesenchymal cells and might limit BMP-driven chondrogenesis.

We next analyzed the Wnt/β-catenin response in LAR family phosphatase-deficient embryos. Interestingly, immunofluorescent labeling for transcriptionally active Ser22/37-dephosphorylated β-catenin (Wu and Pan, 2010) revealed a widespread defect in the mandibular arch of DKO embryos at E10.5. In control mandibular arch active β-catenin signal is apparent in the epithelial and mesenchymal compartments of most of the pharyngeal arch, whereas *Ptprs*$^{-/-}$;*Ptprf*$^{-/-}$ embryos show a significant reduction of β-catenin activity in both compartments, although total β-catenin protein levels are unchanged (Fig. 6A,B; supplementary material Fig. S5A,B). Similarly, *in situ* hybridization for the transcriptional target *Axin2* confirmed the more medial activity of canonical Wnt signaling in control pharyngeal arches, whereas double-mutant embryos exhibited a strong reduction in the extent of *Axin2* expression (Fig. 6C,D). The impairment of Wnt/β-catenin signaling was further confirmed by RT-qPCR analysis of dissected PA1 tissue, which revealed strong downregulation of the canonical target genes *Axin2* and *Ccnd1* in DKO embryos (Fig. 6E).

In MEF cultures, treatment of control cells with recombinant (r) WNT3A resulted in clear localization of β-catenin to the nucleus (Fig. 6F,H). By contrast, LAR family-deficient MEFs retained β-catenin in the cytoplasm upon stimulation with rWNT3A

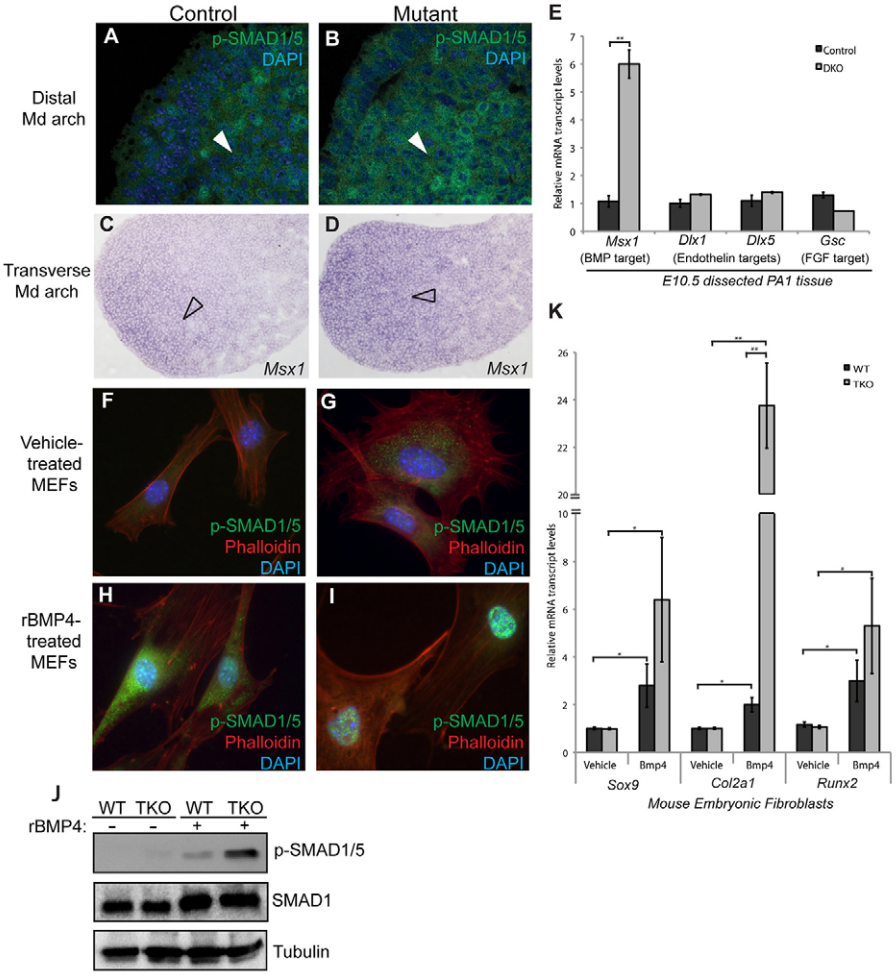

Fig. 5. Increase in Bmp signaling in LAR family phosphatase-deficient cells. (**A**,**B**) Immunofluorescent staining for phosphorylated (p) SMAD1/5 in control (A) and *Ptprs*$^{-/-}$;*Ptprf*$^{-/-}$ (B) mandibular (Md) arches at E10.5. Note the increase in the mesenchymal signal for pSMAD1/5 in the distal mutant arch (arrowhead). (**C**,**D**) *In situ* hybridization for the BMP-regulated gene *Msx1* in control (C) and *Ptprs*$^{-/-}$;*Ptprf*$^{-/-}$ (D) transverse arch sections. Arrowheads indicate the expansion of Msx1 expression in DKO mandibular arch mesenchyme. (**E**) qPCR analysis of dissected control and *Ptprs*$^{-/-}$;*Ptprf*$^{-/-}$ mandibular arches at E10.5 confirms a significant upregulation of *Msx1* upon loss of LAR family phosphatase activity, whereas endothelin and FGF target genes (*Dlx1*, *Dlx5*, *Gsc*) are unaffected. (**F-I**) Immunofluorescent staining for pSMAD1/5 in wild-type (F,H) and *Ptprs*$^{-/-}$;*Ptprf*$^{-/-}$;*Ptprd*$^{-/-}$ triple-knockout (TKO) (G,I) mouse embryonic fibroblasts (MEFs). A specific increase in pSMAD1/5 signal is seen in mutant MEFs upon treatment with recombinant (r) BMP4. (**J**) Western blot analysis of MEFs confirms the specific increase in pSMAD1/5 signal in TKO cells, whereas SMAD1 levels do not differ from wild type (WT). Tubulin provides a loading control. (**K**) qPCR analysis of chondrocyte (*Sox9*, *Col2a1*) and osteoblast (*Runx2*) lineage markers in MEFs upon rBMP4 treatment. Note the stronger upregulation of chondrocytic and osteoblast fates in TKO MEFs. Error bars indicate s.e.; **P*<0.05, ***P*<0.01.

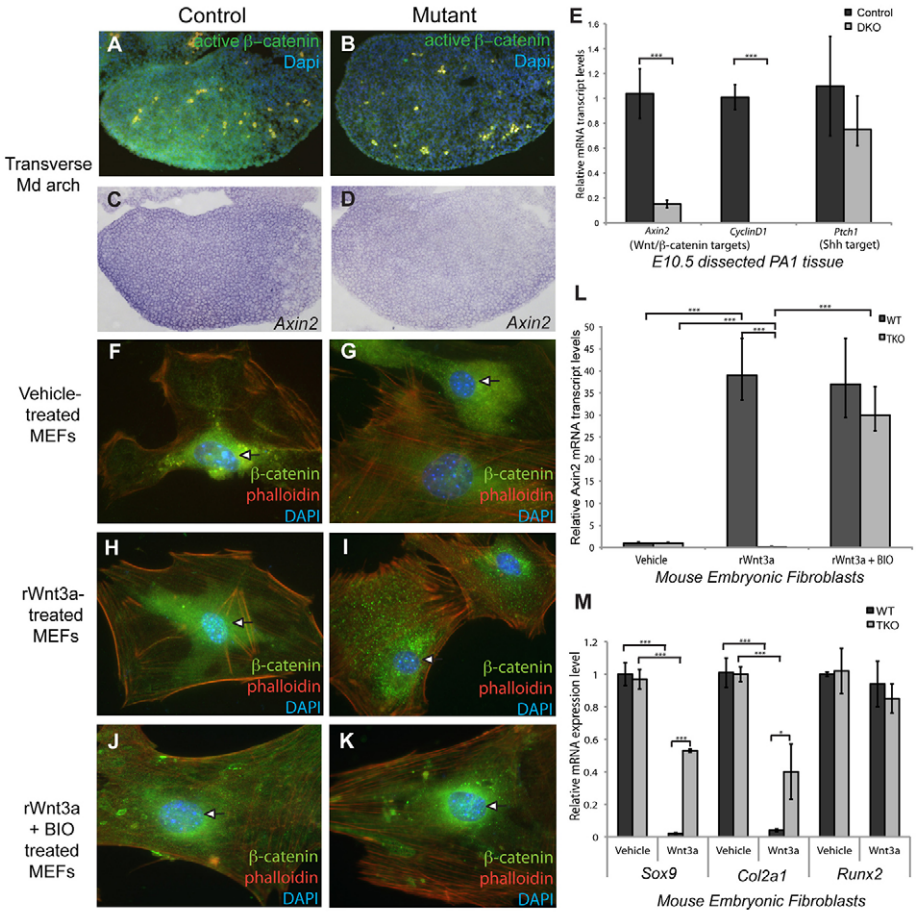

Fig. 6. Decrease in canonical Wnt/β-catenin signaling in cells lacking LAR family phosphatases. (**A**,**B**) Immunofluorescent staining for active β-catenin protein in control (A) and *Ptprs*$^{-/-}$;*Ptprf*$^{-/-}$ (B) transverse mandibular (Md) arch sections at E10.5. A strong downregulation of active β-catenin is observed throughout the mutant mandibular arch. (**C**,**D**) *In situ* hybridization for *Axin2* expression in control (C) and *Ptprs*$^{-/-}$;*Ptprf*$^{-/-}$ (D) mandibular arches. Sections are adjacent to A,B and confirm the loss of canonical Wnt signaling in the mutant. (**E**) qPCR analysis of dissected control and *Ptprs*$^{-/-}$;*Ptprf*$^{-/-}$ mandibular arches at E10.5 reveals significant downregulation of the canonical Wnt target genes *Axin2* and cyclin D1 (*Ccnd1*) in mutant arch tissue. (**F-K**) Immunofluorescent staining for β-catenin in wild-type (F,H,J) and *Ptprs*$^{-/-}$;*Ptprf*$^{-/-}$;*Ptprd*$^{-/-}$ TKO (G,I,K) MEFs. (F-I) β-catenin fails to translocate to the nucleus in mutant MEFs treated with recombinant (r) WNT3A (arrows, F,G). (J,K) Inhibition of GSK3β by the chemical inhibitor BIO restores the nuclear localization of β-catenin protein in TKO MEFs (arrows). (**L**) qPCR analysis of the canonical Wnt target gene *Axin2* reveals the failure of rWNT3A to activate Axin2 transcription in TKO MEFs, which can be rescued by inhibition of GSK3β by BIO. (**M**) qPCR analysis of chondrocyte (*Sox9*, *Col2a1*) and osteoblast (*Runx2*) lineage markers in wild-type versus TKO MEFs upon rWNT3A stimulation. Note the strong repression of chondrocytic fate in wild-type MEFs, which is mitigated by loss of LAR family phosphatase activity. Error bars indicate s.e.; *P<0.01, ***P<0.005.

(Fig. 6G,I). This result was validated with an anti-dephosphorylated Ser22/37 β-catenin antibody that recognizes the active form of β-catenin (Wu and Pan, 2010). Whereas wild-type cells accumulated dephosphorylated nuclear β-catenin, LAR family-deficient cells remained negative for this active form of β-catenin (supplementary material Fig. S5C-F). We next assessed the *Axin2* transcriptional response by qPCR. This revealed a severe impairment in *Axin2* transcriptional activation upon treatment of TKO MEFs with rWNT3A, in sharp contrast to the strong upregulation observed in control MEFs (Fig. 6L). Hence, LAR family-deficient MEFs are refractory to Wnt signaling. This was further confirmed by lineage marker analysis in which rWNT3A treatment of control cells suppressed *Sox9* and *Col2a1* transcription and left the osteoblastic marker *Runx2* unchanged, whereas loss of LAR family activity specifically abrogated the *Sox9*/*Col2a1* chondrocytic response in MEF culture (Fig. 6M).

To further delineate the level at which the LAR phosphatases act on the Wnt/β-catenin pathway, we used the GSK3β inhibitor BIO to prevent β-catenin targeting for proteasome degradation (Meijer et al., 2003). Upon rWNT3A and BIO treatment, TKO MEFs responded to canonical Wnt signaling by both translocating β-catenin to the nucleus and strongly upregulating *Axin2* transcription (Fig. 6J-L). Treatment of TKO cells with BIO alone was unable to stimulate *Axin2* transcription to wild-type levels, confirming the specificity of the response to Wnt signaling (supplementary material Fig. S5G). Together, these results suggest that the LAR family phosphatases act to promote canonical Wnt signaling by relieving the negative regulation of β-catenin, and thereby potentially stimulate proliferative and differentiation responses.

DISCUSSION

Genetic inactivation of the genes encoding the LAR family receptor protein tyrosine phosphatases RPTP-σ and LAR revealed their functional redundancy in craniofacial development. Double-mutant embryos exhibit a shorter lower jaw (micrognathia), accompanied by a failure in tongue development and positioning

(microglossia/glossoptosis) and cleft palate. These defects are caused by a combination of aberrant mandibular patterning and proliferative signaling cues provided by the Wnt and BMP pathways. Importantly, the phenotypic triad of micrognathia, glossoptosis and cleft palate observed in LAR family phosphatase-deficient mice at birth is reminiscent of human PRS.

We previously reported that 45% of DKO embryos harbor micrognathia at E18.5 (Uetani et al., 2009). The basis of this incomplete penetrance is unclear but our results show that the phenotype is already present at E10.5, which implies that the threshold effect on craniofacial morphogenesis occurs prior to this stage. Furthermore, in the present study we found that all *Ptprs;Ptprf* mutants with micrognathia also had microglossia/glossoptosis and cleft palate. Conversely, none of the *Ptprs;Ptprf* mutants without micrognathia had tongue or palate malformations. The strong association between these phenotypes points to a single developmental origin for all three malformations. Since we do not observe early PA1 defects, notably in regard to NCC migration or survival, and as cleft palate or glossoptosis is unlikely to cause micrognathia, the defect in mandibular development is most likely the primary cause of the PRS-like phenotype in DKO embryos. Accordingly, the patterning and proliferation defects occur earlier and are more pronounced in this compartment. The mandibular origin of the PRS triad was also postulated in humans and in previous mouse models (Ricks et al., 2002; Evans et al., 2011). However, as *Ptprf* is also expressed in the palatal epithelium and *Ptprs* is found at lower levels in this region, we cannot exclude the possibility of additional roles for these phosphatases in the maxillary compartment that would sensitize this tissue to palatal shelf defects.

The close resemblance between the LAR family-deficient phenotype and human PRS suggests that the signaling pathways and downstream targets regulated by LAR phosphatases might be involved in PRS etiology. Here, we identified signaling defects in the BMP and Wnt patterning pathways, which have previously been reported to affect mandibular and maxillary development. Of interest, the loss of Wnt pathway components, including LRP6, GSK3β, RSPO2 and β-catenin, results in a variable degree of mandibular hypoplasia and cleft palate linked to altered proliferation and apoptosis (Brault et al., 2001; Song et al., 2009; He et al., 2010; Jin et al., 2011; Sun et al., 2012). Importantly, the severity of jaw abnormality depends upon the timing and the tissue in which β-catenin signaling is blocked (Brault et al., 2001; Sun et al., 2012). Specific loss of β-catenin activity in PA1 results in the distal truncation of Meckel's cartilage, whereas proximal structures remain unaltered, similar to the phenotypes described in *Ptprs;Ptprf* double-mutant embryos (Jin et al., 2011; Zhang et al., 2011; Sun et al., 2012). Furthermore, this phenotype has been linked to proliferation and differentiation defects. Hence, the regulation of Wnt signaling is likely to be an important aspect of LAR family phosphatase function in mandibular development. Interestingly, our results show that GSK3β inhibition is sufficient to restore β-catenin activation and rescue *Axin2* transcription to near wild-type levels upon Wnt stimulation. This suggests that LAR phosphatases regulate the β-catenin degradation complex rather than upstream signal transduction. Further studies will be required to elucidate the detailed mechanism of canonical Wnt/β-catenin regulation by LAR family phosphatases.

In addition to Wnt defects, *Ptprs;Ptprf* mutant mice show an increase in the BMP signaling response. It is intriguing that the aberrant differentiation of Meckel's cartilage that takes place in the LAR family-deficient mandible occurs in the region of increased BMP signaling. BMP4 expression has indeed been demonstrated to upregulate both chondrogenic and osteogenic cell fates (Semba et al., 2000; Yoon et al., 2005; Merrill et al., 2008; Bonilla-Claudio et al., 2012; Kumar et al., 2012). In particular, inducible overexpression of BMP4 results in a shortening of the mandible and expansion of Meckel's cartilage (Bonilla-Claudio et al., 2012). Hence, the increase in BMP signaling in *Ptprs;Ptprf*-deficient embryos is also in line with the observed mandibular phenotype.

Given the concomitant regulation of both the BMP and canonical Wnt signaling pathways by the LAR family phosphatases, one outstanding question concerns the potential for secondary phenotypes due to interaction between the pathways. During PA1 morphogenesis, BMP signaling is active mainly in the distal mandibular mesenchyme (Fig. 5) (Liu et al., 2005; Bonilla-Claudio et al., 2012), while canonical Wnt signaling is detected throughout the proximal-distal axis of the mandibular arch (Fig. 6) (Mani et al., 2010). Hence, based solely on their expression, it is unclear whether these pathways interact in mandibular arch development. However, the fact that simultaneous activation of both the BMP and Wnt pathways in LAR family-deficient fibroblasts was unable to restore SMAD1/5 phosphorylation to wild-type levels and, conversely, that β-catenin activation was unaffected by rBMP4 treatment of wild-type MEFs (data not shown), argues against a secondary phenotype due to pathway interactions. Hence, it is plausible that LAR family phosphatases affect the Wnt and BMP signaling pathways independently and that the combined effect of their misregulation leads to the Meckel's cartilage patterning defects. Our results and those of others (Merrill et al., 2008; Bonilla-Claudio et al., 2012; Kumar et al., 2012) show that mandibular distal BMP promotes cartilage marker gene expression, whereas Wnt signaling represses these genes (Hill et al., 2005; Zhang et al., 2011). In LAR family-deficient cells, the chondrocyte markers *Sox9* and *Col2a1* were strongly activated by BMP signaling, while their repression by Wnt signaling was impaired. This suggests a model in which the combined effect of the misregulation of both pathways impairs cartilage formation in the mandible of *Ptprs;Ptprf* mutant embryos. As a result, bone formation, which requires Meckel's cartilage (Ito et al., 2002), would occur aberrantly (supplementary material Fig. S6). In accordance with a secondary effect on bone formation, loss of LAR family phosphatases had a limited effect on the osteoblast marker *Runx2* in isolated cells. Notably, neither *Ptprs* nor *Ptprf* is expressed in Meckel's cartilage or mandibular bone, supporting a patterning defect rather than a cell-autonomous cartilage or bone differentiation defect.

In addition to patterning defects, the decrease in proliferation observed in double-mutant embryos is likely to exacerbate the mandibular growth phenotype. Proliferation has indeed been identified as a driving force in mandibular elongation (Ito et al., 2002). Proliferation is affected throughout the mandibular region where Wnt/β-catenin signaling is impaired, which correlates with the loss of *Ccnd1* expression, a cell cycle component regulated by Wnt signaling. As the LAR family members are expressed in PA1 mesenchyme at E9.5-10.5, they could directly affect Wnt signaling in these cells to impact proliferation. The later proliferation defects in these tissues might result from the loss of low-level LAR family expression in the more differentiated structures or from secondary mechanisms arising from earlier patterning deficiencies (supplementary material Fig. S6).

In summary, we propose that *Ptprs;Ptprf* double-mutant mice provide important insight into understanding the etiology of PRS, specifically by highlighting the crucial role of mandibular patterning and proliferation control by the Wnt and BMP signaling pathways.

Accordingly, mutations in *BMP2* and in the COL2A1 regulator *SOX9* have been identified in PRS (Snead and Yates, 1999; Benko et al., 2009; Sahoo et al., 2011). These results suggest the LAR family phosphatases as candidate PRS genes in humans and prompt a greater interrogation of the BMP and Wnt pathways in PRS patients.

Acknowledgements
We thank Dr Sami Boualia and Kristen Bertozzi for technical assistance; Dr Z. Kozmik for the *Axin2 in situ* hybridization probe; and the current M.B. laboratory members for helpful discussions and critical review of the manuscript.

Funding
This work was supported by the Canadian Institute for Health Research [MOP-84343 to M.B.]; and by fellowship support from Fonds de la Recherche en Santé du Québec [to K.S.]. M.B. holds a Canada Research Chair in Developmental Genetics.

Competing interests statement
The authors declare no competing financial interests.

Author contributions
K.S. conceived and performed most experiments and wrote the manuscript; N.U. conceived and performed experiments; W.H. provided critical materials; M.L.T. provided critical materials; M.B led the project, conceived the experiments and wrote the manuscript.

Supplementary material
Supplementary material available online at
http://dev.biologists.org/lookup/suppl/doi:10.1242/dev.094532/-/DC1

References

Abu-Issa, R., Smyth, G., Smoak, I., Yamamura, K. and Meyers, E. N. (2002). Fgf8 is required for pharyngeal arch and cardiovascular development in the mouse. *Development* **129**, 4613-4625.
Abzhanov, A. and Tabin, C. J. (2004). Shh and Fgf8 act synergistically to drive cartilage outgrowth during cranial development. *Dev. Biol.* **273**, 134-148.
Benko, S., Fantes, J. A., Amiel, J., Kleinjan, D. J., Thomas, S., Ramsay, J., Jamshidi, N., Essafi, A., Heaney, S., Gordon, C. T. et al. (2009). Highly conserved non-coding elements on either side of SOX9 associated with Pierre Robin sequence. *Nat. Genet.* **41**, 359-364.
Bonilla-Claudio, M., Wang, J., Bai, Y., Klysik, E., Selever, J. and Martin, J. F. (2012). Bmp signaling regulates a dose-dependent transcriptional program to control facial skeletal development. *Development* **139**, 709-719.
Brault, V., Moore, R., Kutsch, S., Ishibashi, M., Rowitch, D. H., McMahon, A. P., Sommer, L., Boussadia, O. and Kemler, R. (2001). Inactivation of the beta-catenin gene by Wnt1-Cre-mediated deletion results in dramatic brain malformation and failure of craniofacial development. *Development* **128**, 1253-1264.
Chagnon, M. J., Uetani, N. and Tremblay, M. L. (2004). Functional significance of the LAR receptor protein tyrosine phosphatase family in development and diseases. *Biochem. Cell Biol.* **82**, 664-675.
Clouthier, D. E., Hosoda, K., Richardson, J. A., Williams, S. C., Yanagisawa, H., Kuwaki, T., Kumada, M., Hammer, R. E. and Yanagisawa, M. (1998). Cranial and cardiac neural crest defects in endothelin-A receptor-deficient mice. *Development* **125**, 813-824.
Elchebly, M., Wagner, J., Kennedy, T. E., Lanctôt, C., Michaliszyn, E., Itié, A., Drouin, J. and Tremblay, M. L. (1999). Neuroendocrine dysplasia in mice lacking protein tyrosine phosphatase sigma. *Nat. Genet.* **21**, 330-333.
Ensslen-Craig, S. E. and Brady-Kalnay, S. M. (2004). Receptor protein tyrosine phosphatases regulate neural development and axon guidance. *Dev. Biol.* **275**, 12-22.
Evans, K. N., Sie, K. C., Hopper, R. A., Glass, R. P., Hing, A. V. and Cunningham, M. L. (2011). Robin sequence: from diagnosis to development of an effective management plan. *Pediatrics* **127**, 936-948.
Funato, N., Chapman, S. L., McKee, M. D., Funato, H., Morris, J. A., Shelton, J. M., Richardson, J. A. and Yanagisawa, H. (2009). Hand2 controls osteoblast differentiation in the branchial arch by inhibiting DNA binding of Runx2. *Development* **136**, 615-625.
Gitton, Y., Heude, E., Vieux-Rochas, M., Benouaiche, L., Fontaine, A., Sato, T., Kurihara, Y., Kurihara, H., Couly, G. and Levi, G. (2010). Evolving maps in craniofacial development. *Semin. Cell Dev. Biol.* **21**, 301-308.
Grote, D., Boualia, S. K., Souabni, A., Merkel, C., Chi, X., Costantini, F., Carroll, T. and Bouchard, M. (2008). Gata3 acts downstream of beta-catenin signaling to prevent ectopic metanephric kidney induction. *PLoS Genet.* **4**, e1000316.
Haapasalo, A., Kim, D. Y., Carey, B. W., Turunen, M. K., Pettingell, W. H. and Kovacs, D. M. (2007). Presenilin/gamma-secretase-mediated cleavage regulates association of leukocyte-common antigen-related (LAR) receptor tyrosine phosphatase with beta-catenin. *J. Biol. Chem.* **282**, 9063-9072.
Haworth, K. E., Wilson, J. M., Grevellec, A., Cobourne, M. T., Healy, C., Helms, J. A., Sharpe, P. T. and Tucker, A. S. (2007). Sonic hedgehog in the pharyngeal endoderm controls arch pattern via regulation of Fgf8 in head ectoderm. *Dev. Biol.* **303**, 244-258.
He, F., Popkie, A. P., Xiong, W., Li, L., Wang, Y., Phiel, C. J. and Chen, Y. (2010). Gsk3β is required in the epithelium for palatal elevation in mice. *Dev. Dyn.* **239**, 3235-3246.
Hendriks, W. J., Elson, A., Harroch, S., Pulido, R., Stoker, A. and den Hertog, J. (2013). Protein tyrosine phosphatases in health and disease. *FEBS J.* **280**, 708-730.
Hill, T. P., Später, D., Taketo, M. M., Birchmeier, W. and Hartmann, C. (2005). Canonical Wnt/beta-catenin signaling prevents osteoblasts from differentiating into chondrocytes. *Dev. Cell* **8**, 727-738.
Hu, D. and Helms, J. A. (1999). The role of sonic hedgehog in normal and abnormal craniofacial morphogenesis. *Development* **126**, 4873-4884.
Hu, D. and Marcucio, R. S. (2009). A SHH-responsive signaling center in the forebrain regulates craniofacial morphogenesis via the facial ectoderm. *Development* **136**, 107-116.
Ishii, M., Han, J., Yen, H. Y., Sucov, H. M., Chai, Y. and Maxson, R. E., Jr (2005). Combined deficiencies of Msx1 and Msx2 cause impaired patterning and survival of the cranial neural crest. *Development* **132**, 4937-4950.
Ito, Y., Bringas, P., Jr., Mogharei, A., Zhao, J., Deng, C. and Chai, Y. (2002). Receptor-regulated and inhibitory Smads are critical in regulating transforming growth factor beta-mediated Meckel's cartilage development. *Dev. Dyn.* **224**. 69-78.
Izumi, K., Konczal, L. L., Mitchell, A. L. and Jones, M. C. (2012). Underlying genetic diagnosis of Pierre Robin sequence: retrospective chart review at two children's hospitals and a systematic literature review. *J. Pediatr.* **160**, 645-650 e2.
Jeong, J., Mao, J., Tenzen, T., Kottmann, A. H. and McMahon, A. P. (2004). Hedgehog signaling in the neural crest cells regulates the patterning and growth of facial primordia. *Genes Dev.* **18**, 937-951.
Jin, Y. R., Turcotte, T. J., Crocker, A. L., Han, X. H. and Yoon, J. K. (2011). The canonical Wnt signaling activator, R-spondin2, regulates craniofacial patterning and morphogenesis within the branchial arch through ectodermal-mesenchymal interaction. *Dev. Biol.* **352**, 1-13.
Kumar, M., Ray, P. and Chapman, S. C. (2012). Fibroblast growth factor and bone morphogenetic protein signaling are required for specifying prechondrogenic identity in neural crest-derived mesenchyme and initiating the chondrogenic program. *Dev. Dyn.* **241**, 1091-1103.
Kypta, R. M., Su, H. and Reichardt, L. F. (1996). Association between a transmembrane protein tyrosine phosphatase and the cadherin-catenin complex. *J. Cell Biol.* **134**, 1519-1529.
Lin, C., Fisher, A. V., Yin, Y., Maruyama, T., Veith, G. M., Dhandha, M., Huang, G. J., Hsu, W. and Ma, L. (2011). The inductive role of Wnt-β-Catenin signaling in the formation of oral apparatus. *Dev. Biol.* **356**, 40-50.
Liu, W., Selever, J., Murali, D., Sun, X., Brugger, S. M., Ma, L., Schwartz, R. J., Maxson, R., Furuta, Y. and Martin, J. F. (2005). Threshold-specific requirements for Bmp4 in mandibular development. *Dev. Biol.* **283**, 282-293.
Machide, M., Hashigasako, A., Matsumoto, K. and Nakamura, T. (2006). Contact inhibition of hepatocyte growth regulated by functional association of the c-Met/hepatocyte growth factor receptor and LAR protein-tyrosine phosphatase. *J. Biol. Chem.* **281**, 8765-8772.
Mackay, D. R. (2011). Controversies in the diagnosis and management of the Robin sequence. *J. Craniofac. Surg.* **22**, 415-420.
Mani, P., Jarrell, A., Myers, J. and Atit, R. (2010). Visualizing canonical Wnt signaling during mouse craniofacial development. *Dev. Dyn.* **239**, 354-363.
McLeod, M. J. (1980). Differential staining of cartilage and bone in whole mouse fetuses by alcian blue and alizarin red S. *Teratology* **22**, 299-301.
Meijer, L., Skaltsounis, A. L., Magiatis, P., Polychronopoulos, P., Knockaert, M., Leost, M., Ryan, X. P., Vonica, C. A., Brivanlou, A., Dajani, R. et al. (2003). GSK-3-selective inhibitors derived from Tyrian purple indirubins. *Chem. Biol.* **10**, 1255-1266.
Merrill, A. E., Eames, B. F., Weston, S. J., Heath, T. and Schneider, R. A. (2008). Mesenchyme-dependent BMP signaling directs the timing of mandibular osteogenesis. *Development* **135**, 1223-1234.
Minoux, M. and Rijli, F. M. (2010). Molecular mechanisms of cranial neural crest cell migration and patterning in craniofacial development. *Development* **137**, 2605-2621.
Müller, T., Choidas, A., Reichmann, E. and Ullrich, A. (1999). Phosphorylation and free pool of beta-catenin are regulated by tyrosine kinases and tyrosine phosphatases during epithelial cell migration. *J. Biol. Chem.* **274**, 10173-10183.
Pfaffl, M. W. (2001). A new mathematical model for relative quantification in real-time RT-PCR. *Nucleic Acids Res.* **29**, e45.

Printzlau, A. and Andersen, M. (2004). Pierre Robin sequence in Denmark: a retrospective population-based epidemiological study. *Cleft Palate Craniofac. J.* **41**, 47-52.
Reid, B. S., Yang, H., Melvin, V. S., Taketo, M. M. and Williams, T. (2011). Ectodermal Wnt/β-catenin signaling shapes the mouse face. *Dev. Biol.* **349**, 261-269.
Ricks, J. E., Ryder, V. M., Bridgewater, L. C., Schaalje, B. and Seegmiller, R. E. (2002). Altered mandibular development precedes the time of palate closure in mice homozygous for disproportionate micromelia: an oral clefting model supporting the Pierre-Robin sequence. *Teratology* **65**, 116-120.
Robin, P. (1934). Glossoptosis due to atresia and hypotrophy of the mandible. *Am. J. Dis. Child.* **48**, 541-547.
Sahoo, T., Theisen, A., Sanchez-Lara, P. A., Marble, M., Schweitzer, D. N., Torchia, B. S., Lamb, A. N., Bejjani, B. A., Shaffer, L. G. and Lacassie, Y. (2011). Microdeletion 20p12.3 involving BMP2 contributes to syndromic forms of cleft palate. *Am. J. Med. Genet. A* **155**, 1646-1653.
Santagati, F. and Rijli, F. M. (2003). Cranial neural crest and the building of the vertebrate head. *Nat. Rev. Neurosci.* **4**, 806-818.
Schaapveld, R. Q., Schepens, J. T., Robinson, G. W., Attema, J., Oerlemans, F. T., Fransen, J. A., Streuli, M., Wieringa, B., Hennighausen, L. and Hendriks, W. J. (1997). Impaired mammary gland development and function in mice lacking LAR receptor-like tyrosine phosphatase activity. *Dev. Biol.* **188**, 134-146.
Schaapveld, R. Q., Schepens, J. T., Bächner, D., Attema, J., Wieringa, B., Jap, P. H. and Hendriks, W. J. (1998). Developmental expression of the cell adhesion molecule-like protein tyrosine phosphatases LAR, RPTPdelta and RPTPsigma in the mouse. *Mech. Dev.* **77**, 59-62.
Semba, I., Nonaka, K., Takahashi, I., Takahashi, K., Dashner, R., Shum, L., Nuckolls, G. H. and Slavkin, H. C. (2000). Positionally-dependent chondrogenesis induced by BMP4 is co-regulated by Sox9 and Msx2. *Dev. Dyn.* **217**, 401-414.
Sheffield, L. J., Reiss, J. A., Strohm, K. and Gilding, M. (1987). A genetic follow-up study of 64 patients with the Pierre Robin complex. *Am. J. Med. Genet.* **28**, 25-36.
Snead, M. P. and Yates, J. R. (1999). Clinical and Molecular genetics of Stickler syndrome. *J. Med. Genet.* **36**, 353-359.
Song, L., Li, Y., Wang, K., Wang, Y. Z., Molotkov, A., Gao, L., Zhao, T., Yamagami, T., Wang, Y., Gan, Q. et al. (2009). Lrp6-mediated canonical Wnt signaling is required for lip formation and fusion. *Development* **136**, 3161-3171.
Stottmann, R. W., Anderson, R. M. and Klingensmith, J. (2001). The BMP antagonists Chordin and Noggin have essential but redundant roles in mouse mandibular outgrowth. *Dev. Biol.* **240**, 457-473.
Sun, Y., Teng, I., Huo, R., Rosenfeld, M. G., Olson, L. E. and Li, X. (2012). Asymmetric requirement of surface epithelial beta-catenin during the upper and lower jaw development. *Dev. Dyn.* **241**, 663-674.
Thomas, T., Kurihara, H., Yamagishi, H., Kurihara, Y., Yazaki, Y., Olson, E. N. and Srivastava, D. (1998). A signaling cascade involving endothelin-1, dHAND and msx1 regulates development of neural-crest-derived branchial arch mesenchyme. *Development* **125**, 3005-3014.
Thompson, K. M., Uetani, N., Manitt, C., Elchebly, M., Tremblay, M. L. and Kennedy, T. E. (2003). Receptor protein tyrosine phosphatase sigma inhibits axonal regeneration and the rate of axon extension. *Mol. Cell. Neurosci.* **23**, 681-692.
Tisi, M. A., Xie, Y., Yeo, T. T. and Longo, F. M. (2000). Downregulation of LAR tyrosine phosphatase prevents apoptosis and augments NGF-induced neurite outgrowth. *J. Neurobiol.* **42**, 477-486.
Uetani, N., Kato, K., Ogura, H., Mizuno, K., Kawano, K., Mikoshiba, K., Yakura, H., Asano, M. and Iwakura, Y. (2000). Impaired learning with enhanced hippocampal long-term potentiation in PTPdelta-deficient mice. *EMBO J.* **19**, 2775-2785.
Uetani, N., Chagnon, M. J., Kennedy, T. E., Iwakura, Y. and Tremblay, M. L. (2006). Mammalian motoneuron axon targeting requires receptor protein tyrosine phosphatases sigma and delta. *J. Neurosci.* **26**, 5872-5880.
Uetani, N., Bertozzi, K., Chagnon, M. J., Hendriks, W., Tremblay, M. L. and Bouchard, M. (2009). Maturation of ureter-bladder connection in mice is controlled by LAR family receptor protein tyrosine phosphatases. *J. Clin. Invest.* **119**, 924-935.
Wallace, M. J., Batt, J., Fladd, C. A., Henderson, J. T., Skarnes, W. and Rotin, D. (1999). Neuronal defects and posterior pituitary hypoplasia in mice lacking the receptor tyrosine phosphatase PTPsigma. *Nat. Genet.* **21**, 334-338.
Wang, X., Weng, L. P. and Yu, Q. (2000). Specific inhibition of FGF-induced MAPK activation by the receptor-like protein tyrosine phosphatase LAR. *Oncogene* **19**, 2346-2353.
Wang, Y., Song, L. and Zhou, C. J. (2011). The canonical Wnt/β-catenin signaling pathway regulates Fgf signaling for early facial development. *Dev. Biol.* **349**, 250-260.
Wu, D. and Pan, W. (2010). GSK3: a multifaceted kinase in Wnt signaling. *Trends Biochem. Sci.* **35**, 161-168.
Yamaguchi, T. P., Bradley, A., McMahon, A. P. and Jones, S. (1999). A Wnt5a pathway underlies outgrowth of multiple structures in the vertebrate embryo. *Development* **126**, 1211-1223.
Yoon, B. S., Ovchinnikov, D. A., Yoshii, I., Mishina, Y., Behringer, R. R. and Lyons, K. M. (2005). Bmpr1a and Bmpr1b have overlapping functions and are essential for chondrogenesis in vivo. *Proc. Natl. Acad. Sci. USA* **102**, 5062-5067.
Yoshida, T., Vivatbutsiri, P., Morriss-Kay, G., Saga, Y. and Iseki, S. (2008). Cell lineage in mammalian craniofacial mesenchyme. *Mech. Dev.* **125**, 797-808.
Zhang, Z., Wlodarczyk, B. J., Niederreither, K., Venugopalan, S., Florez, S., Finnell, R. H. and Amendt, B. A. (2011). Fuz regulates craniofacial development through tissue specific responses to signaling factors. *PLoS ONE* **6**, e24608.
Zhao, Q., Eberspaecher, H., Lefebvre, V. and De Crombrugghe, B. (1997). Parallel expression of Sox9 and Col2a1 in cells undergoing chondrogenesis. *Dev. Dyn.* **209**, 377-386.
Zheng, W., Lennartsson, J., Hendriks, W., Heldin, C. H. and Hellberg, C. (2011). The LAR protein tyrosine phosphatase enables PDGF β-receptor activation through attenuation of the c-Abl kinase activity. *Cell. Signal.* **23**, 1050-1056.

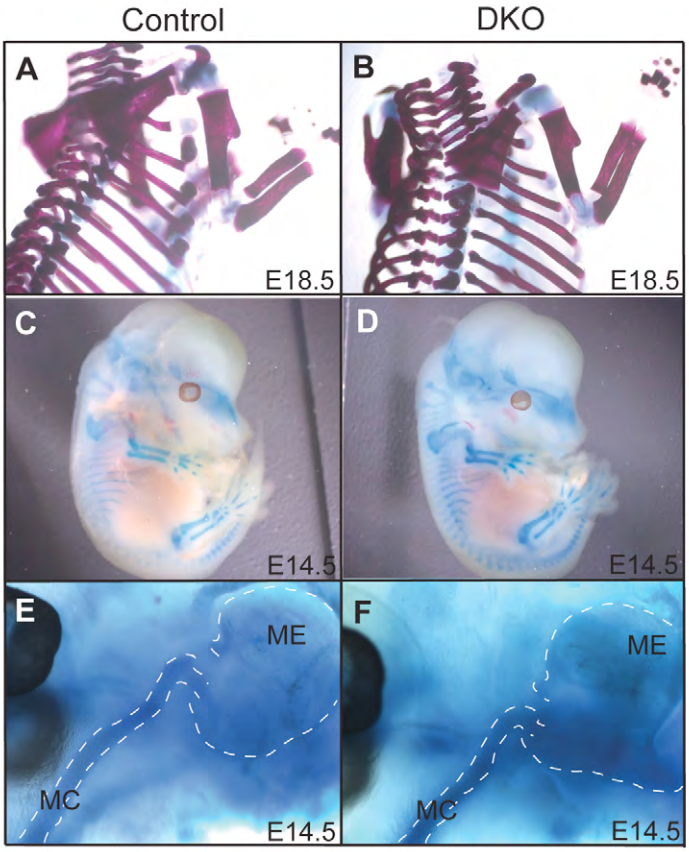

Fig. S1. Appendicular and axial skeletal development is normal in *Ptprs*$^{-/-}$;*Ptprf*$^{-/-}$ embryos. Alizarin Red and Alcian Blue stainings of bone and cartilage. (**A**,**B**) Bone and cartilage development of the DKO body is normal at E18.5. (**C-F**) Bone and cartilage development of the DKO body (C,D) and middle ear capsule (E,F) are normal at E14.5. Note that Meckel's cartilage articulates normally with the middle ear. MC, Meckel's cartilage; ME, middle ear.

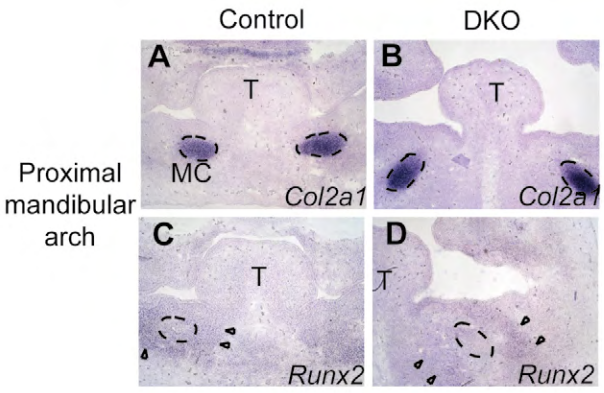

Fig. S2. Proximal Meckel's cartilage is specified normally in *Ptprs*$^{-/-}$;*Ptprf*$^{-/-}$ embryos. (**A-D**) *In situ* hybridization using probes to *Col2a1* and *Runx2* reveals normal proximal Meckel's cartilage specification in DKO mandibular arch at E12.5. Differentiation of proximal bone precursors also occurs normally (arrowheads). MC, Meckel's cartilage; T, tongue.

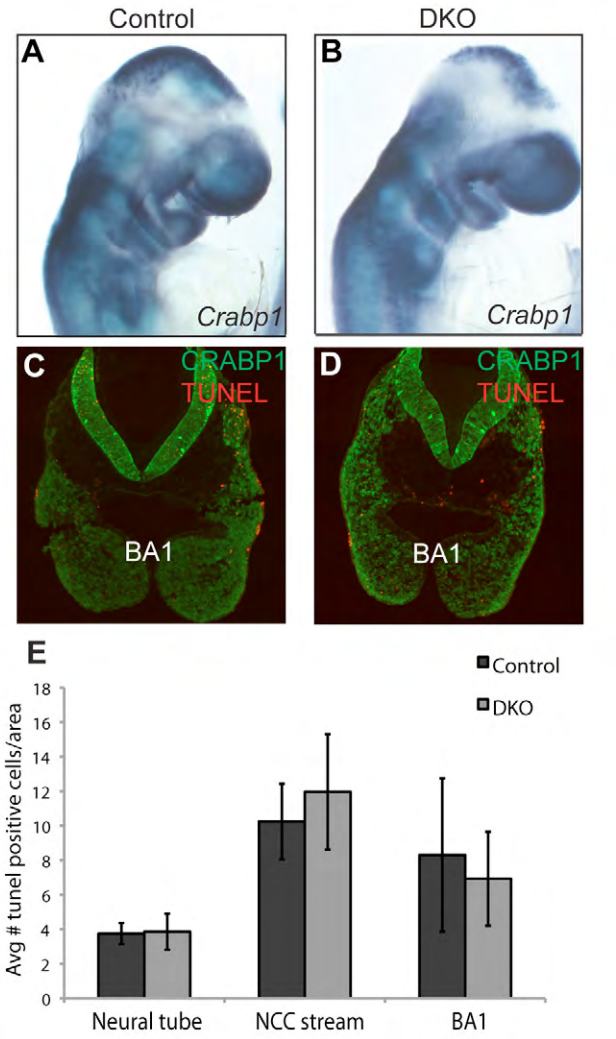

Fig. S3. Neural crest migration and survival in the first branchial arch. (**A**,**B**) Whole-mount *in situ* hybridization using a probe for cellular retinoic acid binding protein (CRABP1) as a marker of migratory neural crest cells reveals normal migration in DKO embryos at E9.5. (**C-E**) Immunofluorescent labeling of CRABP1 and TUNEL reveals no significant difference in neural crest cell (NCC) apoptosis in either the migratory stream or first branchial arch (BA1) at E9.5.

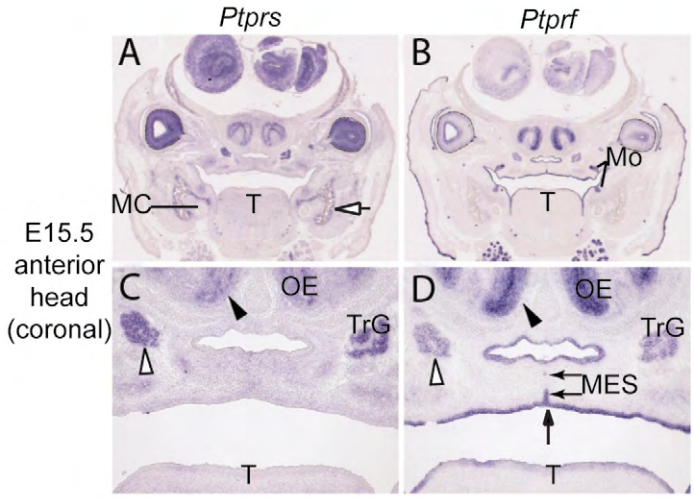

Fig. S4. Expression of *Ptprf* and *Ptprs* during palatal shelf fusion. *In situ* hybridization using probes for *Ptprf* (A,C) and *Ptprs* (B,D) on coronal E15.5 sections. (**A**,**C**) *Ptprf* is expressed in the medial epithelial seam (MES, black arrows) where palatal shelf fusion occurs, as well as throughout the oral epithelium. (**B**,**D**) *Ptprs* is expressed diffusely in the palatal shelf mesenchyme and in ossification centers surrounding Meckel's cartilage (open arrow). Additional regions of strong LAR family expression are indicated by arrowheads. MC, Meckel's cartilage; Mo, molar tooth buds; OE, olfactory epithelium; T, tongue; TrG, trigeminal ganglion.

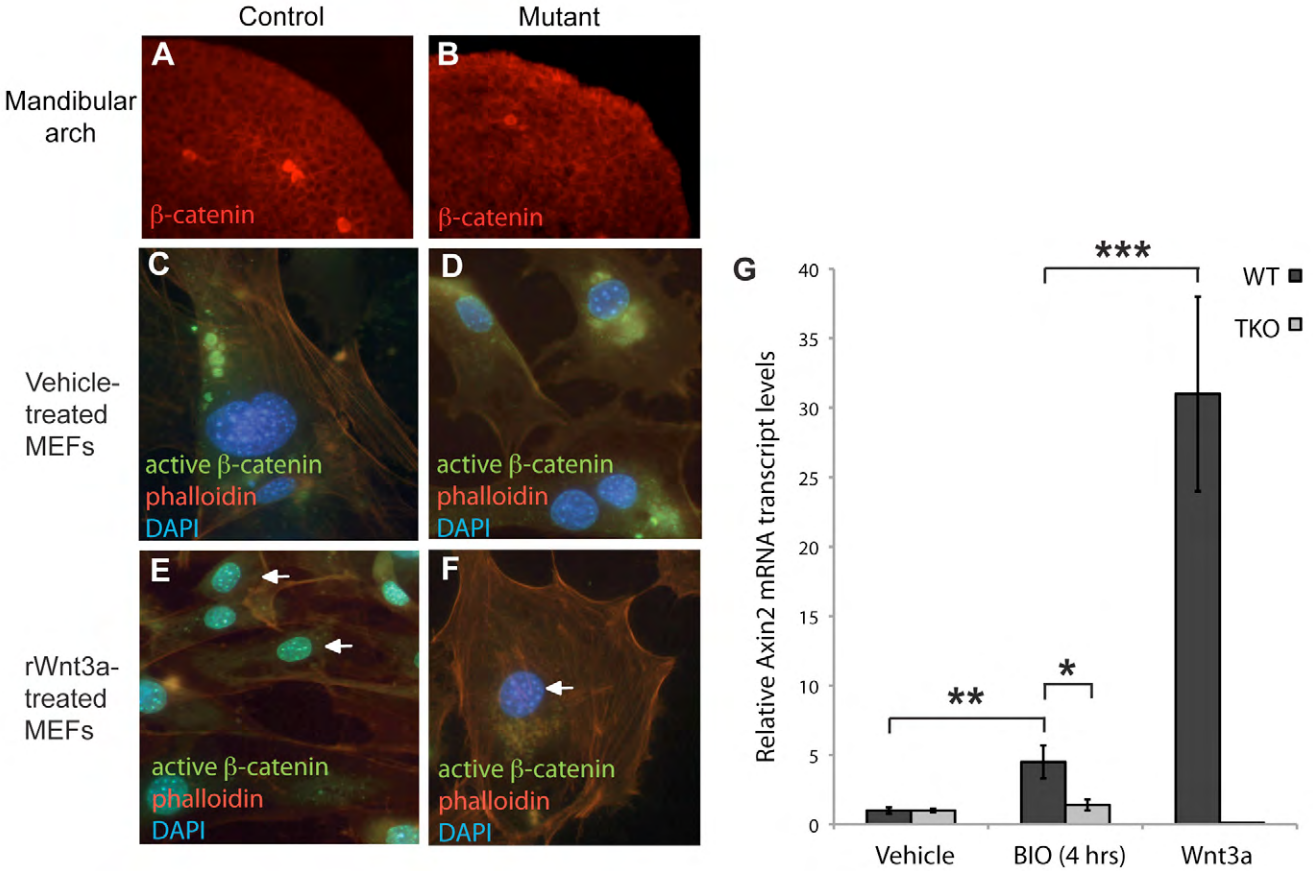

Fig. S5. β-catenin activation is impaired in mouse embryonic fibroblasts mutant for LAR family phosphatase activity. (**A**,**B**) Immunofluorescent staining for total β-catenin protein on coronal E10.5 pharyngeal arch sections. There is no significant difference in β-catenin levels between control (A) and *Ptprs*$^{-/-}$;*Ptprf*$^{-/-}$ (B) embryos. (**C-F**) Immunofluorescent staining of (C,E) wild-type (WT) mouse embryonic fibroblasts (MEFs) and (D,F) *Ptprs*$^{-/-}$;*Ptprf*$^{-/-}$;*Ptprd*$^{-/-}$ triple knockout (TKO) MEFs for Ser27/37 dephosphorylated (active) β-catenin reveals a specific defect in the activation of β-catenin in TKO MEFs upon rWNT3A stimulation (arrows). (**G**) qPCR analysis of *Axin2* transcription reveals that treatment with the GSK3β inhibitor BIO alone is insufficient to restore β-catenin activity, confirming the specificity of the rescue to the Wnt pathway. *P<0.1, **P<0.05, ***P<0.005.

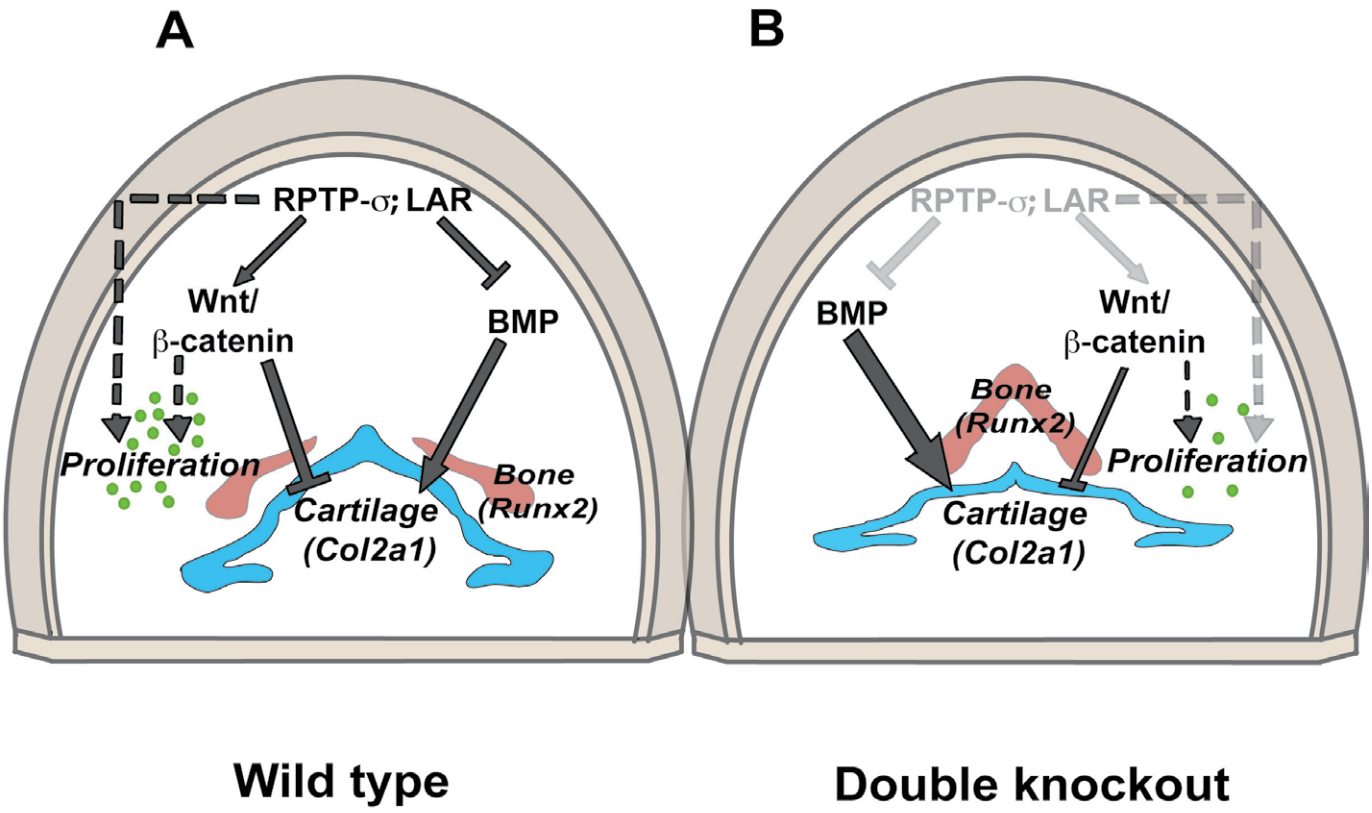

Fig. S6. Model for LAR family phosphatase activity during pharyngeal arch development. (**A**) Normally, PTPRS (RPTPσ) and PTPRF (LAR) act to dampen Bmp signaling activity and promote canonical β-catenin activity, which serves to correctly specify Meckel's cartilage and downstream initiation of mandibular bone development. In addition, PTPRS and PTPRF promote mandibular arch proliferation, potentially through their action on canonical Wnt signaling. (**B**) In *Ptprs*$^{-/-}$;*Ptprf*$^{-/-}$ embryos, loss of the phosphatases permits concomitant intensification of Bmp signaling and downregulation of canonical Wnt restriction of cartilage development, thereby altering the specification of Meckel's cartilage and indirectly affecting mandibular bone positioning. Loss of the LAR family also disrupts proliferation, further affecting mandibular development.

Table S1. Primer sequences for qPCR or ISH

Gene	Use	Forward primer	Reverse primer
beta-microglobin	qPCR	GACTGGTCTTTCTATATCCTGG	CTTTCTGCGTGCATAAATTG
Axin2	qPCR	CCATTTTGGACGACCACCTCTC	GAAGAAGGGTATGACACTGCTGATG
cyclin D1	qPCR	TCTTTCATTGGGCAACGGG	TCCTCAGTTTGGATGGCTCTCC
Ptc1	qPCR	TCTGCTGGGTGTACTGATGC	TCAGGACACGGTCCAAAGA
Msx1	qPCR	TCCTCAAGCTGCCAGAAGAT	TTGGTCTTGTGCTTGCGTAG
Dlx1	qPCR	TTCATCTGACGCTGAGTGTTGG	TTTCCTGTCCTTGTTCCCTCTTC
Dlx5	qPCR	TCAGGAATCGCCAACTTTGC	TGCCATAAGAAGCAGAGGTAGGAG
Gsc	qPCR	TAAGAACCGCCGAGCCAAG	CCGAGTCCAAATCGCTTTTACC
Sox9	qPCR	TCGGAACTGCCTGGAAACTTC	GAGGGAGGGAAAACAGAGAACG
Col2a1	qPCR	GAGCAGCAAGAGCAAGGAAAAG	CAGTGGACAGTAGACGGAGGAAAG
Runx2	qPCR	ACCAGTCTTACCCCTCCTATCTGAG	GCAGTGTCATCATCTGAAATACGC
Msx1	ISH	CCTACGCAAGCACAAGACCAAC	TGGGGACCACGGATAAATCTC
Col2a1	ISH	CATTATTGACATCGCACCC	CAGAATAGCACCATTGTGTAGG
Runx2	ISH	GAGCTATTAAAGTGACAGTGGACGG	CAACACCATCATTCTGGTTAGGC
Crabp1	ISH	CAGCAGAGGTGGGTGCCTGCCC	GCAGCCAACCAGTTTAATGACTGG

All primers are shown 5' to 3'.